This article is published as part of the *Dalton Transactions* themed issue entitled:

Coordination chemistry in the solid state

Guest Editor Russell E. Morris

Published in Issue 14, Volume 41 of *Dalton Transactions*

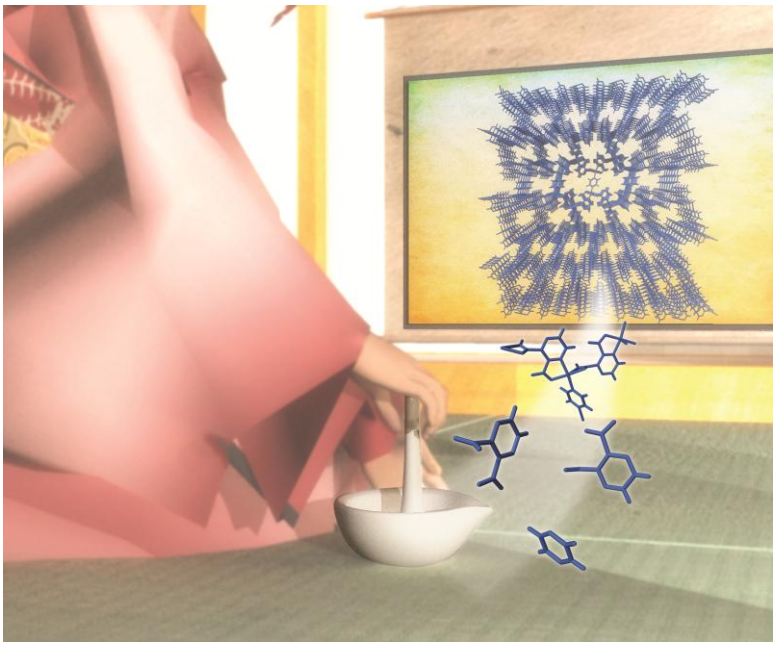

Articles in this issue include:

Communications

Highly oriented surface-growth and covalent dye labeling of mesoporous metal–organic frameworks
Florian M. Hinterholzinger, Stefan Wuttke, Pascal Roy, Thomas Preuße, Andreas Schaate, Peter Behrens, Adelheid Godt and Thomas Bein

Papers

Supramolecular isomers of metal–organic frameworks: the role of a new mixed donor imidazolate-carboxylate tetradentate ligand
Victoria J. Richards, Stephen P. Argent, Adam Kewley, Alexander J. Blake, William Lewis and Neil R. Champness

Hydrogen adsorption in the metal–organic frameworks Fe_2(dobdc) and $Fe_2(O_2)$(dobdc)
Wendy L. Queen, Eric D. Bloch, Craig M. Brown, Matthew R. Hudson, Jarad A. Mason, Leslie J. Murray, Anibal Javier Ramirez-Cuesta, Vanessa K. Peterson and Jeffrey R. Long

Visit the *Dalton Transactions* website for the latest cutting inorganic chemistry
www.rsc.org/publishing/journals/dt/

Dalton Transactions

Dynamic Article Links

Cite this: *Dalton Trans.*, 2012, **41**, 4180

www.rsc.org/dalton

PAPER

Hydrogen adsorption in the metal–organic frameworks Fe_2(dobdc) and $Fe_2(O_2)$(dobdc)†

Wendy L. Queen,[a,b] Eric D. Bloch,[b] Craig M. Brown,*[a,c] Matthew R. Hudson,[a,d] Jarad A. Mason,[b] Leslie J. Murray,[b,e] Anibal Javier Ramirez-Cuesta,[f] Vanessa K. Peterson[c] and Jeffrey R. Long*[b]

Received 8th November 2011, Accepted 11th January 2012
DOI: 10.1039/c2dt12138g

The hydrogen storage properties of Fe_2(dobdc) (dobdc^{4-} = 2,5-dioxido-1,4-benzenedicarboxylate) and an oxidized analog, $Fe_2(O_2)$(dobdc), have been examined using several complementary techniques, including low-pressure gas adsorption, neutron powder diffraction, and inelastic neutron scattering. These two metal–organic frameworks, which possess one-dimensional hexagonal channels decorated with unsaturated iron coordination sites, exhibit high initial isosteric heats of adsorption of −9.7(1) and −10.0 (1) kJ mol^{-1}, respectively. Neutron powder diffraction has allowed the identification of three D_2 binding sites within the two frameworks, with the closest contacts corresponding to Fe–D_2 separations of 2.47(3) and 2.53(5) Å, respectively. Inelastic neutron scattering spectra, obtained from *p*-H_2 (*para*-H_2) and D_2–*p*-H_2 mixtures adsorbed in Fe_2(dobdc), reveal weak interactions between two neighboring adsorption sites, a finding that is in opposition to a previous report of possible 'pairing' between neighboring H_2 molecules.

Introduction

As a substitute for diminishing fossil fuels, hydrogen stands at the forefront among alternative energy carriers due to its high gravimetric energy content and clean combustion. One of the greatest obstacles to a hydrogen economy is the current lack of a safe, efficient, and economically viable on-board storage technology that would enable a driving range similar to those of gasoline powered automobiles. Due to their high internal surface areas, adjustable pore sizes, and chemical tunability, metal–organic frameworks are being investigated as potential hydrogen storage materials. While many frameworks have the ability to store significant amounts of H_2 at 77 K, their utility in the temperature range of interest, −40 °C to 60 °C,[1] is hampered by weak dispersive type interactions, which are characterized by adsorption enthalpies ranging from −4 to −7 kJ mol^{-1}.[2] As a result, at room temperature, they often show little to no improvement in storage density relative to the compression of pure H_2 gas.

From a structural standpoint, several factors, such as pore size, surface area, catenation, and ligand functionalization, can significantly affect the hydrogen storage characteristics of a metal–organic framework.[3] In order to facilitate H_2 adsorption at higher temperatures it is evident that stronger binding interactions are required. Theoretical calculations predict that for significant storage capacity near room temperature frameworks will require isosteric heats of adsorption to be between −15 and −25 kJ mol^{-1}.[4] Recent research has shown that the incorporation of coordinatively-unsaturated metal centers into the frameworks can provide both enhanced binding energy[5] and an increase in the surface packing density of adsorbates at low temperature.[6]

Compounds of the type M_2(dobdc) (M = Mg, Mn, Fe, Co, Ni, Zn; dobdc^{4-} = 2,5-dioxido-1,4-benzenedicarboxylate), also commonly referred to as M-MOF-74 or CPO-27-M, constitute an isostructural family of metal–organic frameworks with one-dimensional hexagonal channels.[7] The framework walls consist of helical chains of oxo- and carboxylato-bridged M^{2+} cations interlinked through dobdc^{4-} ligands. Upon thermal activation of the framework, a bound solvent molecule is liberated from each pseudo-octahedral M^{2+} cation, leaving an open coordination site that points directly into one of the channels. These highly-reactive, electron-deficient sites allow for strong polarization of incoming H_2 molecules that bind to the framework surface, leading to zero-coverage isosteric heats ranging from −8.8 to −13.5 kJ mol^{-1}.[6,7e,8] These values are among the largest reported to date and show significant improvement over the

[a]*National Institute of Standards and Technology, Center for Neutron Research, Gaithersburg, MD20899, USA. E-mail: craig.brown@nist.gov*
[b]*Department of Chemistry, University of California, Berkeley and Division of Materials Sciences, Lawrence Berkeley National Laboratory, Berkeley, CA94720, USA. E-mail: jrlong@berkeley.edu; Tel: +5106420860*
[c]*The Bragg Institute, Australian Nuclear Science and Technology Organisation, Lucas Heights, NSW 2234, Australia*
[d]*Department of Materials Science and Engineering, University of Maryland, College Park, MD20742, USA*
[e]*Department of Chemistry, University of Florida, Gainesville, FL32611, USA*
[f]*ISIS Facility, Rutherford Appleton Laboratory, Chilton, Didcot, Oxon, OX11 0QX, UK*

†Electronic supplementary information (ESI) available: Crystallographic information, Inelastic neutron scattering spectra, 87 K H_2 uptake data, and plots showing isosteric heats for H_2 adsorption. CCDC reference numbers 853659–853664. For ESI and crystallographic data in CIF or other electronic format see DOI: 10.1039/c2dt12138g

isosteric heats of H_2 adsorption observed for frameworks lacking exposed metal cation sites.[2]

While a number of metal–organic frameworks incorporating iron(II)[9] or iron(III)[10] have been reported, their preparation remains a relative rarity. Furthermore, the gas adsorption properties of only a very few such compounds featuring open metal coordination sites have been studied.[9c,d,10c,d] Herein, we report the hydrogen storage characteristics of the redox-active metal–organic framework Fe_2(dobdc) and its oxidized counterpart $Fe_2(O_2)$(dobdc). The combination of H_2 adsorption studies with neutron scattering measurements affords important insight into the H_2 loading characteristics of the materials, allowing us to draw correlations between binding energy and M–D_2 distances for the homologous M_2(dobdc) series.

Experimental

The syntheses of Fe_2(dobdc) and $Fe_2(O_2)$(dobdc) were carried out using previously published procedures.[11] Prior to data collection, the samples were activated under dynamic vacuum at 433 K for 18 h. Low-pressure N_2 adsorption data result in a Langmuir surface area of approximately 1535 $m^2\ g^{-1}$ (1360 $m^2\ g^{-1}$ Brunauer–Emmett–Teller (BET)) for Fe_2(dobdc) and 1150 $m^2\ g^{-1}$ for $Fe_2(O_2)$(dobdc).[11]

Low-pressure gas adsorption measurements

A 200 mg sample of Fe_2(dobdc)·4MeOH was transferred to a pre-weighed glass sample tube under a N_2 atmosphere and capped with a Transeal. The sample was then transferred to a Micromeritics ASAP 2020‡ gas adsorption analyzer and heated at a rate of 0.1 K min^{-1} to 433 K while under vacuum. The sample was considered activated when the outgas rate at 433 K was less than 2 μbar min^{-1}. The evacuated tube containing the degassed sample was then transferred to a balance and weighed to determine the mass of the sample (≈150 mg). The tube was then transferred to the analysis port of the instrument, where the outgas rate was again determined to be less than 2 μbar min^{-1} at 433 K. The N_2 gas adsorption isotherm at 77 K was measured in liquid N_2, while H_2 measurements were carried out at 77 K in liquid N_2 and also at 87 K using liquid Ar. A 94.4 mg sample of $Fe_2(O_2)$(dobdc) was treated similarly.

Neutron powder diffraction

Neutron powder diffraction (NPD) experiments were carried out on 0.9698 g of activated Fe_2(dobdc) using the high-resolution neutron powder diffractometer, BT1, at the National Institute of Standards and Technology Center for Neutron Research (NCNR). The sample was placed in a He purged glove box, loaded into a vanadium can equipped with a gas loading valve, and sealed using an In O-ring. NPD data were collected using a Ge(311) monochromator with an in-pile 60′ collimator corresponding to a wavelength of 2.0782 Å. The sample was loaded into a top-loading closed cycle refrigerator and data were collected on the bare framework at 4 K. For D_2 loading, the sample was warmed to 80 K and then exposed to a predetermined amount of D_2. Upon reaching an equilibrium pressure at the loading temperature, the sample was then slowly cooled to ensure equilibrium and complete adsorption of the D_2. Data were collected at 4 K for loadings of 0.75 and 2.25 D_2 molecules per iron. For the oxidized derivative, $Fe_2(O_2)$(dobdc) (0.620 g), data were collected on the bare framework at 4 K followed by sequential loadings of 0.25, 0.5, 1.0, and 2.0 D_2 molecules per iron.

Additional NPD measurements of D_2-loaded Fe_2(dobdc) were performed on the high-intensity neutron powder diffractometer, WOMBAT,[12] located at the OPAL reactor facility at the Australian Nuclear Science and Technology Organisation (ANSTO). An activated 1.076 g sample of Fe_2(dobdc) was transferred to a vanadium can in an Ar-filled glovebox. The cell was equipped with heaters for the gas line and valve to allow rapid and uniform temperature control. Wombat was configured with a Ge (113) monochromator with a take-off angle of 110° with open primary and secondary collimation, resulting in a $La^{11}B_6$ (NIST Standard 660b) calibrated wavelength of 2.7948 Å. Data were collected at select temperatures upon cooling. Temperatures ranged between 300 K and 10 K for the bare Fe_2(dobdc) framework and below 100 K for sequential loadings of 0.5, 1.0, 1.5, and 2.0 D_2 molecules per iron. For each loading, the cryostat and sample were heated to 100 K to perform adsorption of the D_2 gas.

All NPD data were analyzed using the Rietveld method as implemented in EXPGUI/GSAS.[13] The activated Fe_2(dobdc) model was refined with all structural and peak profile parameters free to vary, resulting in a structure very similar to that previously determined.[11] Fourier difference methods were then employed to locate the adsorbed D_2 molecules in the data collected from the samples subsequently loaded with D_2. The D_2 molecules were modeled as double occupancy atoms due to quantum mechanical rotations that make the molecules almost spherical.[14] For data obtained from the oxidized sample, $Fe_2(O_2)$(dobdc), the modeled O atoms were constrained to maintain the same fractional occupancies and isotropic atomic displacement parameters (ADPs). Once a stable structural model was obtained, the isotropic ADPs of the chemisorbed O_2 molecule were allowed to vary independently of one another, with the ADPs for O(1b) refined anisotropically in order to effectively capture the disorder at this site.

Inelastic neutron scattering

Inelastic neutron scattering (INS) experiments were performed on 0.467 g and 0.620 g of Fe_2(dobdc) and $Fe_2(O_2)$(dobdc), respectively, employing the Filter Analyzer Neutron Spectrometer (FANS) at the NCNR.[15] Spectra were obtained by illuminating the samples with a collimated, and monochromated neutron beam. After passing through a low-energy band-pass filter consisting of Bi, Be, and graphite, the energy transfer of the scattered neutrons was determined at a bank of ^{3}He detectors. Data were first collected for the bare framework, followed by

‡ Certain trade names and company products are mentioned in this paper to adequately specify the experimental procedure and equipment used. In no case does this imply recommendation or endorsement by NIST, nor does it imply that the products are necessarily the best available for this purpose.

data collection for frameworks loaded with *normal*-H_2 (*n*-H_2). It should be noted that *n*-H_2 contains a 3 : 1 mixture of *ortho* (*o*-H_2) and *para* (*p*-H_2) hydrogen, respectively. For Fe_2(dobdc), data were collected for loadings of 0.1, 0.25, 0.5, 1.0, and 1.5 *n*-H_2 molecules per iron, while for $Fe_2(O_2)$(dobdc) data were collected for loadings of 0.5, 1.0, and 1.5 *n*-H_2 molecules per iron. Gas was loaded into the framework using the same methods as described for the high-resolution NPD experiments. The spectra of the bare frameworks were then subtracted from the spectra obtained from the H_2 loaded samples using the DAVE suite of programs.[16]

Additional INS experiments were carried out on 1.347 g of Fe_2(dobdc) using the TOSCA[17] neutron spectrometer located at the ISIS facility of the Rutherford Appleton Laboratories. The instrument allowed us to probe energy transfers between 2 and 500 meV, and in this region the instrument has a resolution of ≈2% $\Delta E/E$. The gas loadings, consisting of 0.5, 1.0, 2.25, 3.0, and 3.75 *p*-H_2 molecules per iron were carried out using methods similar to those previously described. The *p*-H_2 was prepared in a separate cryostat using a magnetic catalyst and low-temperature H_2. Further experiments were carried out on Fe_2(dobdc), where the sample was first loaded with 1.0 D_2 molecules per iron followed by sequential *p*-H_2 loadings of 0.5, 1.25, 2.0, and 2.75 *p*-H_2 molecules per iron at 30 K. This approach allowed saturation of the metal sites with the much weaker scattering D_2, enabling an easier determination of spectral lines associated with the weaker H_2 adsorption sites.

Results and discussion

H_2 adsorption isotherms

Fig. 1 shows the low-pressure excess H_2 uptake at 77 K for an activated sample of Fe_2(dobdc). The uptake quickly reaches an adsorption above 1 wt% at the very low pressure of 6 mbar. Although H_2 binding is physisorptive in nature, the steep initial rise in the isotherm is indicative of the presence of very strongly polarizing sites. Additionally, a large internal surface area leads to an uptake of approximately 2.2 wt% at 1.2 bar.

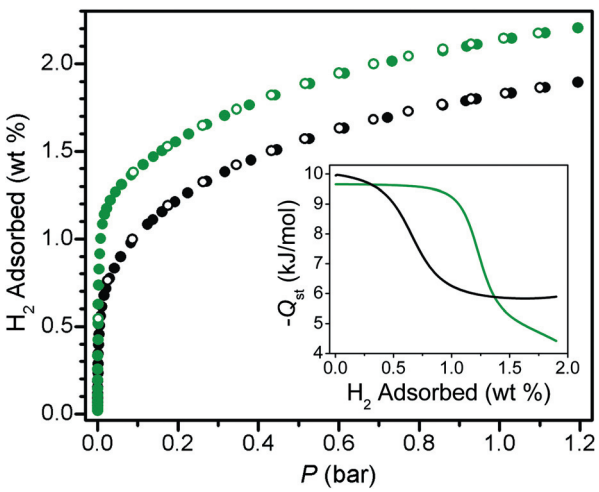

Fig. 1 Excess H_2 adsorption isotherms collected for Fe_2(dobdc) (green) and $Fe_2(O_2)$(dobdc) (black) at 77 K. Filled and open circles represent adsorption and desorption, respectively. Inset: Isosteric heats of adsorption ($-Q_{st}$) plotted as a function of adsorbed H_2 for both Fe_2(dobdc) (green) and $Fe_2(O_2)$(dobdc) (black).

In order to calculate isosteric heats of adsorption (Q_{st}) as a function of loading using the Clausius–Clapeyron equation, it is first required to accurately determine the precise pressures that correspond to identical loadings of H_2 for at least two temperatures.[18] As such, it is necessary to use a model to fit the experimental isotherm adsorption data. The calculation of Q_{st} is particularly sensitive to the accuracy of the fit to the experimental data, especially when very strong adsorption sites are present. Here, the isosteric heats of adsorption were determined for Fe_2(dobdc) by three different methods: fitting the 77 and 87 K isotherm data simultaneously with a virial-type equation, fitting the 77 and 87 K data independently with a virial-type equation, and fitting the 77 and 87 K data independently with a dual-site Langmuir isotherm (see ESI† for details).[19] Significantly, only the dual-site Langmuir model was able to adequately model the inflection that occurs in the isotherms as saturation of the open Fe^{2+} sites is approached. It should be noted that this fitting method gives rather different, and we believe more accurate, results than the virial-type fitting procedure that has typically been used for analyzing such data.

Using a dual-site Langmuir fitting of the 77 and 87 K data, the low-coverage isosteric heat ($-Q_{st}$) of H_2 adsorption was determined to be −9.7(1) kJ mol^{-1} (see Fig. 1, inset), a value similar to that observed for H_2 in Mg_2(dobdc).[20,21] At uptakes above 1.3 wt% the isosteric heat drops below −7 kJ mol^{-1}, which is typical of materials featuring weak dispersive type interactions between the adsorbed gas and framework and is consistent with saturation of the strong Fe^{2+} adsorption sites within the material.

By gradually dosing O_2 at room temperature, Fe_2(dobdc) can be controllably oxidized to an iron(III)-containing derivative, $Fe_2(O_2)$(dobdc). We have previously shown that 50% of the open coordination sites of the Fe^{3+} cations within this compound are occupied by a peroxide (O_2^{2-}) species, while the other 50% remain open.[11] It was expected that the higher charge density of Fe^{3+} (ionic radii for Fe^{2+} = 0.78 Å and Fe^{3+} = 0.64 Å)[22] would lead to an overall stronger binding, a direct result of increased polarization of the adsorbed gas. Indeed, this is likely the case, given the observed zero-coverage Q_{st} value of −10.0(1) kJ mol^{-1} (see Fig. 1, inset), which is comparable to Fe_2(dobdc) despite the availability of only half as many metal cation binding sites. The lower number of strong binding sites further leads to a significant drop in the magnitude of Q_{st} for $Fe_2(O_2)$(dobdc) at loadings higher than 0.25 wt%. Accordingly, the excess H_2 uptake data at 1.2 bar is only approximately 1.9 wt% at 77 K. This significant reduction in the low-pressure storage capacity can further be justified when considering the reduction in surface area by a ∼25% decrease based on Langmuir surface areas of 1535 m^2 g^{-1} and 1150 m^2 g^{-1} for Fe_2(dobdc) and $Fe_2(O_2)$ (dobdc), respectively, together with the slightly higher molecular weight (∼10%) of $Fe_2(O_2)$(dobdc).

Neutron diffraction data

In order to obtain a better understanding of the site specific binding properties of these materials, detailed powder neutron

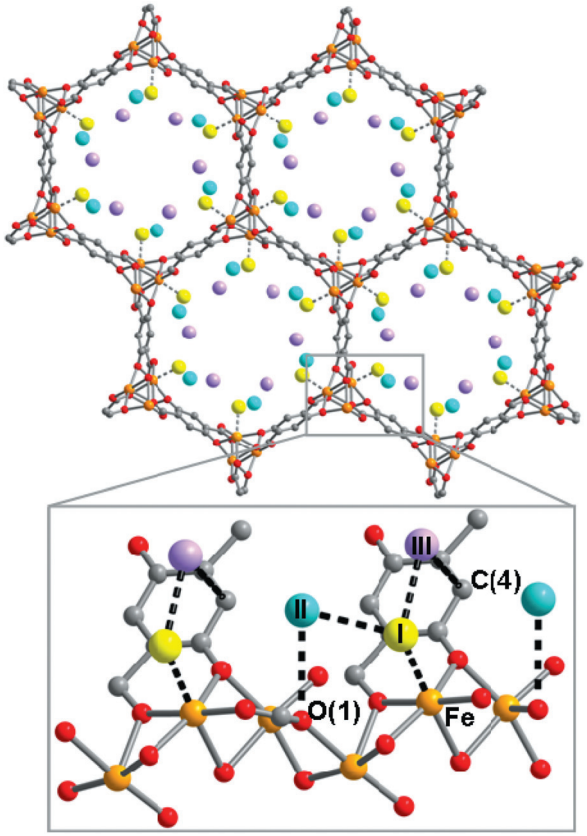

Fig. 2 $Fe_2(dobdc)$ loaded with 2.25 D_2 per Fe^{2+}, viewed along the [001] direction. Orange, gray, red spheres represent Fe, C, and O atoms, respectively. The box contains a close up view of the framework wall, showing closest D_2–D_2 and D_2–framework interactions (drawn as dotted lines) along the channel. Three D_2 sites, determined by neutron powder diffraction, are labeled as I, II, and III in order of binding strength.

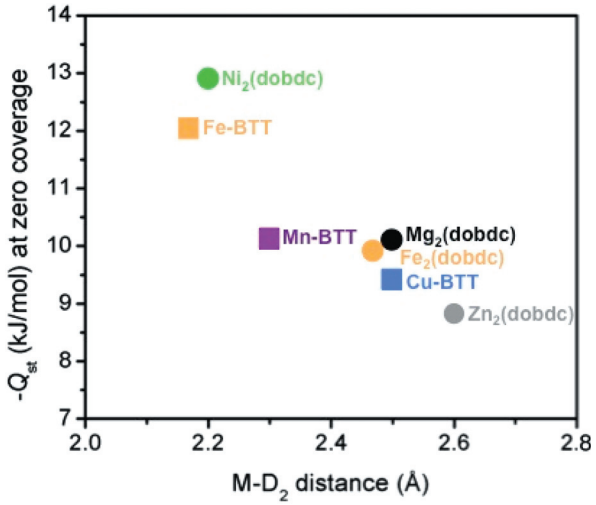

Fig. 3 Isosteric heats ($-Q_{st}$) plotted as a function of M–D_2 distances for two metal–organic framework families including M_2(dobdc)[6,18] and M-BTT.[5d,e,10c]

diffraction experiments were performed, allowing us to probe structural changes in the framework as well as the exact positions, occupancies, and site affinities of adsorbed D_2 molecules. Rietveld refinement using the diffraction data obtained for the bare Fe_2(dobdc) is well described using a structural model similar to the one previously published.[11] After structural refinement of the host material, Fourier difference maps allowed subsequent elucidation of the D_2 positions and site occupancies as a function of D_2 loading. Development of a suitable structural model permitted nearly unconstrained Rietveld refinements.

The diffraction data (BT1, NCNR) for Fe_2(dobdc), dosed with approximately 0.75 D_2 molecules per iron, indicate the population of a position, site I, located 2.47(3) Å from the open metal center (see Fig. 2). This confirms that the unsaturated metal cation is responsible for the high initial isosteric heat of adsorption. Although few metal–organic framework families exhibiting extensive chemical substitution at the metal site have been studied using neutron diffraction, there is a correlation for isosteric heats and M–D_2 distances observed within two families reported thus far (see Fig. 3), including M_2(dobdc) and M-BTT (BTT^{3-} = 1,3,5-benzenetristetrazolate, M = Mn, Fe, Cu).[5d,e,6,10c,20] It is shown that compounds with similar isosteric heats yet different structure types, as in the case of Mn-BTT[5e] and Mg_2(dobdc),[20] do not necessarily display similar M–D_2 distances, illustrating the importance of the local framework structure and the metal ligation. However, within the isostructural M_2(dobdc) series, variants featuring Mg^{2+} and Fe^{2+} exhibit M–D_2 distances and calculated zero-coverage Q_{st} values that are the same within error,[20] while the Zn^{2+} analog has a much longer M–D_2 distance of ~2.60 Å, corresponding to a zero-coverage Q_{st} of just −8.8 kJ mol^{-1}.[6] First principles calculations based on density-functional theory (DFT) have been used to qualitatively determine M–D_2 distances in the M_2(dobdc) series and revealed a fair correlation between the calculated values, ionic radii of the M^{2+} cations, and zero-coverage Q_{st} values.[7e]

Upon loading the Fe_2(dobdc) with 2.25 D_2 molecules per iron, two additional sites become populated, labeled as II and III in Fig. 2. These sites are similar to those observed in the Zn^{2+} analog,[6] and display approximate intermolecular separations that range from 2.87 to 3.22 Å while the closest framework to D_2 contacts lie in the range from 3.2 to 3.3 Å. These observations indicate that intermolecular D_2 interactions are similar in strength to those of the physisorptive interactions with the framework surface. Relative to site I, the large atomic displacement parameters observed for sites II and III are typical of weakly bound adsorbates.

Rapid collection of diffraction data, obtained from a high-intensity neutron powder diffractometer (WOMBAT, ANSTO), was used to assess structural changes in the framework as a function of loading and temperature. At a low loading there is essentially a temperature independent occupation of D_2 at the open metal (see Fig. S2†). After dosing the sample with 1.0 D_2 molecule per iron, the data begins to reveal occupation of site II, with a population factor of ~0.2; this trend continues with site II occupation increasing until near saturation in the highest loading of 2.0 D_2 molecules per Fe^{2+}. Fourier difference maps indicate no population of site III up to a dosing of 2.0 D_2 molecules per iron, demonstrating a lower adsorption enthalpy for that position. This result is consistent with previous investigations of Zn_2(dobdc), which include data from various techniques such as

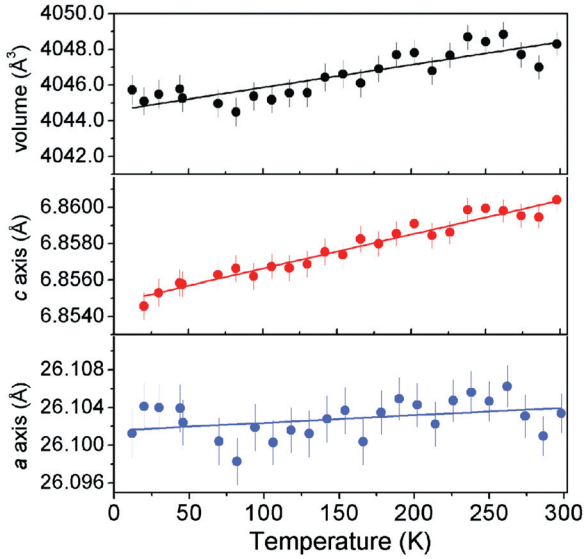

Fig. 4 Unit cell parameters of the bare Fe_2(dobdc) framework plotted as a function of increasing temperature. The data were acquired using a high-intensity powder neutron diffractometer, Wombat. The lines represent a linear fit to the data with the error bars representing a single standard deviation.

diffraction[6] and both neutron and infrared spectroscopies.[23] While the 0.5 and 1.0 loading levels reveal little change in binding site occupancies upon heating up to 100 K, the 1.5 and 2.0 loadings show a more significant depopulation of site II.

The unit cell volume of Fe_2(dobdc) at 10 and 100 K is plotted as a function of D_2 loading in Fig. S3.† The data reveal that, at constant temperature, there is an expansion in the unit cell with higher D_2 loading. Surprisingly, however, at constant coverage, observed in the 0.25 and 0.5 loadings, there is a statistically significant compression of the unit cell with increasing temperature. While 10 to 100 K is a relatively small temperature range over which to investigate thermal properties, given the limited resolution and Q range of the instrument, the data suggest negative thermal expansion. In order to investigate this further, we performed diffraction experiments on the bare framework over a wider range of temperatures. The material exhibits only a slight expansion in unit cell volume between 10 K and 300 K (see Fig. 4), with a volume expansivity of $3.2(4) \times 10^{-6}$ K^{-1}. The majority of the expansivity is derived from the *c*-axis ($2.5(2) \times 10^{-6}$ K^{-1}), whereas there is almost no thermal expansion along the *a* and *b* axes ($3.1(6) \times 10^{-7}$ K^{-1}). This indicates that the negative thermal expansion observed for the D_2-adsorbed Fe_2(dobdc) structure between 10 K and 100 K is in some way associated with hydrogen binding. The diffraction data do not allow a clear determination of the mechanism for the observed thermal properties, as the changes in the overall unit cell are minimal. It is evident that much of the negative thermal expansion reported in metal–organic frameworks thus far has been attributed to dynamic properties related to low-energy vibrational modes found within the frameworks,[24] making the current influence of the fairly weakly bound molecule even more striking.

Neutron diffraction experiments (BT1, NCNR) were also carried out on $Fe_2(O_2)$(dobdc). An initial loading of 0.25 D_2 molecules per iron indicates population of only site I with a Fe–D_2 distance of 2.53(5) Å, similar to the case in Fe_2(dobdc) and consistent with the large zero-coverage Q_{st} value. At a loading of 0.5 D_2 molecules per iron, the atomic displacement parameters for site I increase significantly, indicative of D_2 disorder close to the open metal coordination site. In an effort to model the disorder, site I was further split into two crystallographically-independent molecular units. While there was an improvement in the refinement, one D_2 molecule remains fairly disordered. The observed static disorder at site I could result from two phenomena: (i) a nonuniform distribution of the strongly binding O_2^{2-} species on the framework surface, likely causing some short range disorder with respect to the Fe^{3+} environments and (ii) physisorptive interactions occurring between D_2 molecules and the bound peroxide species, which displays large displacement parameters for O(1b). While both circumstances could cause inadequacies in our ability to completely model the data using the current technique, the 1.0 and 2.0 D_2 molecules per iron loadings give experimental support of a secondary D_2 binding in close proximity to the peroxide species, as site I D_2 occupancies are significantly higher than 0.5. Even though the site I $D_2\cdots O_2^{2-}$ distances are short, they are not discussed further due to the extensive site I disorder making it difficult to determine any detailed atomic information. Also, in comparison to Fe_2(dobdc), there is a significant reduction in magnitude for Q_{st} at H_2 loadings above 0.25 wt%, likely due to the weaker (O_2^{2-})–D_2 interaction, since it is expected that peroxide bound sites would be less polarizing than the exposed metal cation.

Increasing loadings from 1.0 to 2.0 D_2 molecules per iron results in a sequential occupation of sites II and III, as observed for the parent Fe_2(dobdc) compound; however, as in the case of the open metal site, the refined thermal parameters for II and III are large relative to those observed in the Fe^{2+} analog. While they are susceptible to a larger error, a consequence of increased static disorder, intermolecular D_2 distances range from ~2.7 to ~3.0 Å, while the closest framework$\cdots D_2$ interactions lie between 3.2 Å and 3.3 Å for sites II and III. The D_2 molecules adsorbed at site II also reveal weak van der Waals type interactions with the bound peroxide species, with a separation of ~3.0 Å from O(1b).

Inelastic neutron scattering spectra

Inelastic neutron scattering experiments were also utilized to probe the site specific binding properties of H_2. In solid H_2, where the molecules behave as three-dimensional quantum rotors, the energy levels (E_J) for each rotational level (J) can be described by $E_J = BJ(J+1)$, where B is the rotational constant equal to 7.35 meV. Therefore, the transition from $J = 0$ to $J = 1$, also known as the *para* to *ortho* transition, occurs at an energy of 2B or 14.7 meV, in ideal H_2. Adsorption of H_2 at relatively high enthalpy sites can create a barrier to the quantum rotation, resulting in a shift in the observed rotational lines from 14.7 meV. Additionally, anisotropic environments, with respect to the local framework surrounding adsorption sites, can lift the degeneracy of the triplet $J = 1$ state, causing splitting of the 14.7 meV peak into separate entities.

Selected INS spectra obtained (FANS, NIST) for Fe_2(dobdc) loaded with 0.1 to 1.5 *n*-H_2 molecules per iron after subtraction

of the bare spectrum are shown in Fig. S4.† At low loadings of 0.1 to 0.5 *n*-H_2 molecules per iron, there are two observable rotational lines centered at ≈6.1 and ≈11.5 meV with additional features between 20 and 30 meV. Similar transitions have been observed in the INS spectra for members of the M_2(dobdc) series with M = Zn, Ni, Co, Mg.[20,21,23a] The two lowest energy peaks and the ≈22 meV peak have been previously assigned, by INS measurements that were correlated with diffraction results[23a] and subsequently confirmed through DFT calculations,[25] as transitions occurring from the $J = 0$ state to three sublevels of the split $J = 1$ rotational state. It is evident that Fe_2(dobdc) exhibits the largest splitting observed thus far for a member of this family of compounds. Further, within this series, the size of the splitting and peak positions show no correlation with strength of binding at the open metal site.[26]

Additional INS spectra of Fe_2(dobdc) with various loadings ranging from 0.5 to 3.75 *p*-H_2 molecules per iron were measured on the TOSCA spectrometer at ISIS. The neutron energy loss spectra, ranging from 2 to 125 meV, is shown in Fig. S5† (after subtraction of the bare framework spectrum). The intensity obtained at higher energy transfers on TOSCA is less than that of FANS, due to the different quantities measured on each spectrometer.[14] The spectra obtained for the sample loaded with *n*-H_2 (FANS) gives qualitatively the same spectral features as those obtained using *p*-H_2 (TOSCA) indicating that *ortho–para* conversion happens in *n*-H_2 upon adsorption into Fe_2(dobdc). The total scattering in these spectra is proportional to the number of H_2 molecules in the system, including the rotational transitions and background associated with recoil effects of the H_2 molecules. The results from integrating the total intensity for each data set correlate very well with the loadings for each experiment (see Fig. S6†).

Fig. 5 shows the INS data obtained from TOSCA over a smaller energy range, 2 meV to 20 meV, in order to highlight the low-energy rotational transitions observed for the three adsorption sites. At loadings above 1.0 H_2 molecules per iron, as sites

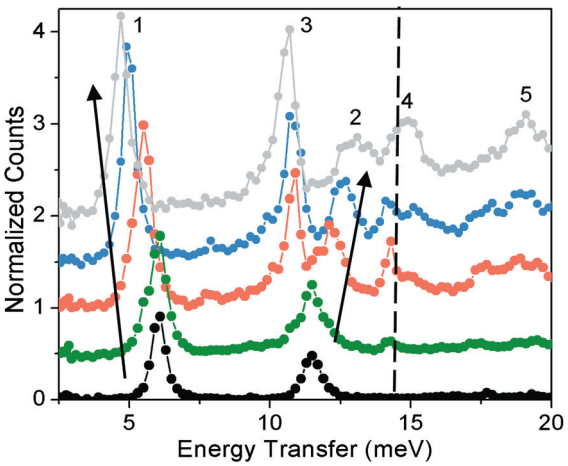

Fig. 5 INS spectra at 20 K for loadings of 0.5 (black), 1.0 (green), 2.25 (orange), 3.0 (blue), and 3.75 (grey) *p*-H_2 per Fe^{2+} in Fe_2(dobdc). The data shown are after subtraction of the spectrum of the evacuated framework. All rotational lines, especially those associated with site I (denoted by arrows), shift as a function of loading. The dashed line, at 14.7 meV, represents the *o–p* transition of bulk H_2.

II and III are populated, the additional molecules are close enough to each other to affect the rotational potential at site I, and this consequently adjusts the rotational energy level, as seen in the shift of peak 1 to lower frequencies and peak 2 to higher frequencies. This lowest frequency line shifts by almost 1.4 meV over the entire loading range, much more than was observed for the other members of the M_2(dobdc) series, which have shown only small effects on the lowest rotational transition (on the order of 0.2 meV). The magnitude of this shift is similar to that observed between the gas phase and solid bulk hydrogen,[27] a scenario that is very different from the present situation within Fe_2(dobdc).

A recent combined infrared spectroscopy and DFT theory study of M_2(dobdc) (M = Mg, Co, Ni, Zn) suggested that there is a 'pairing' of the H_2 molecules between the first and the second adsorption sites, and that the second adsorption site is only stable if there is population on the unsaturated metal.[28] A significant portion of this inference comes from the close H_2–H_2 distance of 2.6 Å, a value that was misquoted from our previous work, in which the distances in question are actually ~2.9 to 4.2 Å. The average intermolecular distance, 3.4 Å, is shorter than the distance found in solid D_2, 3.6 Å, yet it does not constitute a criterion to label these adsorbates as paired. Indeed, the pairing description misinterprets the temperature dependence of the INS spectra, which illustrates the decreasing population of the separate adsorption sites as a consequence of differing adsorption enthalpies. The behavior of the site occupancies as a function of temperature (see Fig. S2†) also supports the traditional view that these are essentially independent adsorption sites, as site II shows a much stronger temperature dependence than the much higher-enthalpy site I. If indeed there is H_2–H_2 pairing, the use of both D_2 and H_2 in our INS studies should enable the observation of a transition from the paired to the unpaired state, as it would have an effect on the rotational energy levels of this newly associated super-molecule as also indicated by the large shifts in vibrational frequency.[28]

To highlight the rotational transitions observed for H_2 at sites II and III we masked the site I transitions in the INS spectra by dosing the sample with 1 D_2 molecule per iron (see Fig. 6). Due to the lower zero-point motion and entropy, the D_2 will bind to the metal preferentially over H_2. A further dosing of the sample with *p*-H_2 yields spectra with contributions from only the weaker adsorption sites, II and III, due to the large difference in the incoherent cross section for hydrogen *versus* deuterium: 80.26 and 2.05 barns, respectively. The use of *p*-H_2 is important in this case as it is likely that conversion to the ground-state cannot occur easily with access to the Fe^{2+} blocked, and we wish to directly compare populations in each rotational state. Comparing the spectra obtained from the samples loaded with 1.5 *p*-H_2 to the 1.0 D_2 + 0.5 *p*-H_2 dosing clearly reveals two peaks associated with site II at approximately 10.6 and 14.2 meV, respectively (peaks labeled 3 and 4), enabling a clear assignment of peaks 1 and 2 to the rotational levels of H_2 bound at the open metal site. An additional dosing of 1.25 *p*-H_2 to the sample with 1.0 D_2 molecules per iron yields a spectrum with a broad feature around 15.0 meV that must originate from H_2 at site III, similar to the energy expected for almost unhindered H_2 rotations and indicating more weakly bound H_2. It is evident that there is little difference between the spectra obtained for pure *p*-H_2 and those

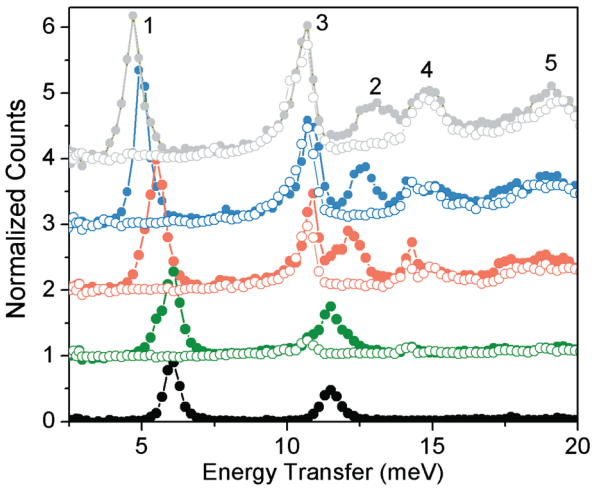

Fig. 6 INS spectra at 20 K for $Fe_2(dobdc)$ loaded with various amounts of *p*-H_2 (closed circles) and 1.0 D_2 molecule per Fe^{2+} + various amounts of *p*-H_2 (open circles). The material was loaded with 0.5 (black circles), 1.5 (green circles), 2.25 (orange circles), 3.0 (blue circles), and 3.75 (grey circles) gas molecules per Fe^{2+}. The data shown are after subtraction of the spectrum of the evacuated framework.

obtained for the D_2–*p*-H_2 mixtures, so we conclude that the H_2–H_2 and D_2–H_2 'pairs' have similar rotational levels and hence the interactions between sites I and II must be weak.

INS was also used to probe the H_2 rotational transitions in $Fe_2(O_2)(dobdc)$ (see Fig. S7†). While there is some peak broadening observed for the dosings (0.5, 1.0, and 1.5 *n*-H_2 molecules per iron), likely due to the aforementioned static disorder, the spectra for both the oxidized and unoxidized compounds look extremely similar. The rotational transitions observed for all loadings have similar intensities, indicating analogous H_2 occupancies between the materials. It is expected that if 50% of the open metal cation sites are blocked by the presence of O_2^{2-} upon dosing with H_2 the intensities of the rotational transitions associated with sites II and III would increase more rapidly for $Fe_2(O_2)(dobdc)$ than for $Fe_2(dobdc)$. The fact that the intensities remain the same supports H_2 population in close proximity to the peroxide bound sites, as supported by the diffraction data. Similar peak positions also indicates a similar rotational barrier for H_2 molecules interacting with the metal, as well as those interacting with the peroxide, despite a relatively weaker adsorption enthalpy for the latter.

Conclusions

Gas adsorption measurements coupled with neutron diffraction and spectroscopy has provided an unambiguous image of the mechanism for hydrogen storage properties of the newest member of the $M_2(dobdc)$ family. While the H_2 uptake properties of $Fe_2(dobdc)$ closely mirror those of $Mg_2(dobdc)$, studies of this kind offer structure–property correlations that are necessary to pinpoint the structural factors that affect the isosteric heat of H_2 adsorption within metal–organic frameworks, and allow us to test the accepted idea that shorter metal–adsorbate bond distances lead to an increased adsorption enthalpy. Employing inelastic neutron scattering spectroscopy, we have confirmed that rotational transitions associated with H_2 bound at the open metal site do not necessarily correlate with binding energies. These experiments have further provided a conclusive demonstration that 'pairing' of H_2 molecules at two neighboring adsorption sites does not occur in this system. In addition, the INS data coupled with neutron diffraction has revealed the first experimental evidence of D_2 binding to a peroxide-containing species, as observed in $Fe_2(O_2)(dobdc)$. Although the electrostatic interaction at the peroxide appears to be somewhat weaker than the open metal, it is still significantly stronger than typical van der Waals interactions traditionally observed in these frameworks. It is expected that continued systematic studies of this family as well as other metal–organic frameworks will inform the design of next-generation hydrogen storage materials.

Note added in proof

We would like to point out a partial investigation of hydrogen adsorption in $Fe_2(dobdc)$ that came to our attention after submission of this article.[29]

Acknowledgements

This research was funded by was funded by the Department of Energy under Contract No. DE-AC02-05CH11231. In addition, work at NIST was partially supported by the Office of Energy Efficiency and Renewable Energy (EERE). We acknowledge fellowship support for W.L.Q. from the NIST/NRC Fellowship Program and for J.A.M. from the National Science Foundation. We thank Prof. C. J. Kepert for the use of an inert atmosphere glovebox, and M. Kibble and C. Goodway from ISIS for their help in gas loading experiments performed on TOSCA. We are also grateful to the neutron scattering facilities, ISIS, ANSTO, and NIST NCNR, for allocating the beamtime necessary to carry out these experiments.

References

1 EERE: Fuel Cell Technologies Program http://www.eere.energy.gov/hydrogenandfuelcells, accessed October 2011.
2 B. Schmitz, U. Müller, N. Trukhan, M. Schubert, G. Férey and M. Hirscher, *ChemPhysChem*, 2008, **9**, 2181.
3 (*a*) J. L. C. Rowsell and O. M. Yaghi, *Angew. Chem., Int. Ed.*, 2005, **44**, 4647; (*b*) X. Lin, J. Jia, X. Zhao, K. M. Thomas, A. J. Blake, G. S. Walker, N. R. Champness, P. Hubberstey and M. Schröder, *Angew. Chem., Int. Ed.*, 2006, **45**, 7358; (*c*) D. J. Collins and H.-C. Zhou, *J. Mater. Chem.*, 2007, **17**, 3154; (*d*) L. J. Murray, M. Dincă and J. R. Long, *Chem. Soc. Rev.*, 2009, **38**, 1294; (*e*) J. Yang, A. Sudik, C. Wolverton and D. J. Siegel, *Chem. Soc. Rev.*, 2010, **39**, 656.
4 (*a*) S. K. Bhatia and A. L. Myers, *Langmuir*, 2006, **22**, 1688; (*b*) E. Garrone, B. Bonelli and C. O. Areán, *Chem. Phys. Lett.*, 2008, **456**, 68; (*c*) Y.-S. Bae and R. Q. Snurr, *Microporous Mesoporous Mater.*, 2010, **132**, 300.
5 (*a*) B. Chen, N. W. Ockwig, A. R. Millward, D. S. Contreras and O. M. Yaghi, *Angew. Chem., Int. Ed.*, 2005, **44**, 4745; (*b*) S. S. Kaye and J. R. Long, *J. Am. Chem. Soc.*, 2005, **127**, 6506; (*c*) A. G. Wong-Foy, A. J. Matzger and O. M. Yaghi, *J. Am. Chem. Soc.*, 2006, **128**, 3494; (*d*) M. Dincă, A. Dailly, Y. Liu, C. M. Brown, D. A. Neumann and J. R. Long, *J. Am. Chem. Soc.*, 2006, **128**, 16876; (*e*) M. Dincă, W. S. Han, Y. Liu, A. Dailly, C. M. Brown and J. R. Long, *Angew. Chem., Int. Ed.*, 2007, **46**, 1419; (*f*) D. Britt, D. Tranchemontagne and O. M. Yaghi, *Proc. Natl. Acad. Sci. U. S. A.*, 2008, **105**, 11623; (*g*) M. Dincă and J. R. Long, *Angew. Chem., Int. Ed.*, 2008, **47**, 6766; (*h*) H. Wu, W. Zhou and T. Yildirim, *J. Am. Chem. Soc.*, 2009, **131**, 4995; (*i*) S. Ma, D. Yuan, J.-

S. Chang and H.-C. Zhou, *Inorg. Chem.*, 2009, **48**, 5398; (*j*) X. Lin, I. Telepeni, A. J. Blake, A. Dailly, C. M. Brown, J. M. Simmons, M. Zoppi, G. S. Walker, K. M. Thomas, T. J. Mays, P. Hubberstey, N. R. Champness and M. Schröder, *J. Am. Chem. Soc.*, 2009, **131**, 2159.

6 Y. Liu, H. Kabbour, C. M. Brown, D. A. Neumann and C. C. Ahn, *Langmuir*, 2008, **24**, 4772.

7 (*a*) N. L. Rosi, J. Kim, M. Eddaoudi, B. Chen, M. O'Keeffe and O. M. Yaghi, *J. Am. Chem. Soc.*, 2005, **127**, 1504; (*b*) P. D. C. Dietzel, Y. Morita, R. Blom and H. Fjellvåg, *Angew. Chem., Int. Ed.*, 2005, **44**, 6354; (*c*) P. D.C. Dietzel, B. Panella, M. Hirscher, R. Blom and H. Fjellvåg, *Chem. Commun.*, 2006, 959; (*d*) S. R. Caskey, A. G. Wong-Foy and A. J. Matzger, *J. Am. Chem. Soc.*, 2008, **130**, 10870; (*e*) W. Zhou, H. Wu and T. Yildirim, *J. Am. Chem. Soc.*, 2008, **130**, 15268; (*f*) P. D. C. Dietzel, R. E. Johnsen, R. Blom and H. Fjellvåg, *Chem.–Eur. J.*, 2008, **14**, 2389; (*g*) P. D. C. Dietzel, R. Blom and H. Fjellvåg, *Eur. J. Inorg. Chem.*, 2008, 3624; (*h*) S. Bhattacharjee, J. S. Choi, S. T. Yang, S. B. Choi, J. Kim and W. S. Ahn, *J. Nanosci. Nanotechnol.*, 2010, **10**, 135.

8 J. G. Vitillo, L. Regli, S. Chavan, G. Ricchiardi, G. Spoto, P. D. C. Dietzel, S. Bordiga and A. Zecchina, *J. Am. Chem. Soc.*, 2008, **130**, 8386.

9 (*a*) T. R. Whitfield, X. Wang, L. Liu and A. J. Jacobson, *Solid State Sci.*, 2005, **7**, 1096; (*b*) S. Bauer, C. Serre, T. Devic, P. Horcajada, J. Marrot, G. Férey and N. Stock, *Inorg. Chem.*, 2008, **47**, 7568; (*c*) P. Horcajada, S. Surblé, C. Serre, D.-Y. Hong, Y.-K. Seo, J.-S. Chang, J.-M. Grenèche, I. Margiolaki and G. Férey, *Chem. Commun.*, 2007, 2820; (*d*) A. Fateeva, S. Devautour-Vinot, N. Heymans, T. Devic, J.-M. Grenèche, S. Wuttke, S. Miller, A. Lago, C. Serre, G. De Weireld, G. Maurin, A. Vimont and G. Férey, *Chem. Mater.*, 2011, **23**, 4641.

10 (*a*) G. J. Halder, K. W. Chapman, S. M. Neville, B. Moubaraki, K. S. Murray, J.-F. Létard and C. J. Kepert, *J. Am. Chem. Soc.*, 2008, **130**, 17552; (*b*) S. Ma, D. Yuan, J.-S. Chang and H.-C. Zhou, *Inorg. Chem.*, 2009, **48**, 5398; (*c*) K. Sumida, S. Horike, S. S. Kaye, Z. R. Herm, W. L. Queen, C. M. Brown, F. Grandjean, G. J. Long, A. Dailly and J. R. Long, *Chem. Sci.*, 2010, **1**, 184; (*d*) D. Lupu, O. Ardelean, G. Blanita, G. Borodi, M. D. Lazar, A. R. Biris, C. Ioan, M. Mihet, I. Misan and G. Pepeneciu, *Int. J. Hydrogen Energy*, 2011, **36**, 3586.

11 E. D. Bloch, L. J. Murray, W. L. Queen, S. Chavan, S. N. Maximoff, J. P. Bigi, R. Krishna, V. K. Peterson, F. Grandjean, G. J. Long, B. Smit, S. Bordiga, C. M. Brown and J. R. Long, *J. Am. Chem. Soc.*, 2011, **133**, 14814.

12 A. J. Studer, M. E. Hagen and T. J. Noakes, *Phys. B*, 2006, **385–386**, 1013.

13 (*a*) A. C. Larson and R. B. Von Dreele, 'General Structure Analysis System (GSAS)', Los Alamos National LaboratoryReport LAUR, 1994, p. 86 (*b*) B. H. Toby, EXPGUI, a graphical user interface for GSAS, *J. Appl. Crystallogr.*, 2001, **34**, 210.

14 C. M. Brown, Y. Liu, T. Yildirim, V. K. Peterson and C. J. Kepert, *Nanotechnology*, 2009, **20**, 204025.

15 T. J. Udovic, C. M. Brown, J. B. Leão, P. C. Brand, R. D. Jiggetts, R. Zeitoun, T. A. Pierce, I. Peral, J. R. D. Copley, Q. Huang, D. A. Neumann and R. J. Fields, *Nucl. Instrum. Methods Phys. Res., Sect. A*, 2008, **588**, 406.

16 R. T. Azuah, L. R. Kneller, Y. Qiu, P. L. W. Tregenna-Piggott, C. M. Brown, J. R. D. Copley and R. M. Dimeo, *J. Res. Natl. Inst. Stand. Technol.*, 2009, **114**, 241.

17 (*a*) S. F. Parker, C. J. Carlile, T. Pike, J. Tomkinson, R. J. Newport, C. Andreani, F. P. Ricci, F. Sacchetti and M. Zoppi, *Phys. B*, 1998, **154**, 241; (*b*) D. Colognesi, M. Celli, F. Cilloco, R. J. Newport, S. F. Parker, V. Rossi-Albertini, F. Sacchetti, J. Tomkinson and M. Zoppi, *Appl. Phys. A: Mater. Sci. Process.*, 2002, **74**, s64; (*c*) P. C. H. Mitchell, S. F. Parker, A. J. Ramirez-Cuesta and J. Tomkinson, *Vibrational Spectroscopy with Neutrons with Applications in Chemistry, Biology, Material Sciences and Catalysis*, World Scientific, Singapore, 2005.

18 B. Chen, X. Zhao, A. Putkham, K. Hong, E. B. Lobkovsky, E. J. Hurtado, A. J. Fletcher and K. M. Thomas, *J. Am. Chem. Soc.*, 2008, **130**, 6411.

19 (*a*) L. Czepirski and J. Jagiełło, *Chem. Eng. Sci.*, 1989, **44**, 797; (*b*) S. Sircar, *Ind. Eng. Chem. Res.*, 1992, **31**, 1813.

20 K. Sumida, C. M. Brown, Z. R. Herm, S. Chavan, S. Bordiga and J. R. Long, *Chem. Commun.*, 2011, **47**, 1157.

21 P. D. C. Dietzel, P. A. Georgiev, J. Eckert, R. Blom, T. Strässle and T. Unruh, *Chem. Commun.*, 2010, **46**, 4962.

22 R. D. Shannon, *Acta Crystallogr., Sect. A: Cryst. Phys., Diffr., Theor. Gen. Crystallogr.*, 1976, **32**, 751.

23 (*a*) Y. Liu, C. M. Brown, D. A. Neumann, H. Kabbour and C. C. Ahn, in *Life Cycle Analysis for New Energy Conversion and Storage Systems*, ed. V. M. Fthenakis, A. C. Dillon and N. Savage, (Mater. Res. Soc. Symp. Proc., Volume 1041E, Warrendale, PA), 2008, 1040-R2_03; (*b*) S. A. FitzGerald, J. Hopkins, B. Burkholder, M. Friedman and J. L. C. Rowsell, *Phys. Rev. B: Condens. Matter Mater. Phys.*, 2010, **81**, 104305.

24 (*a*) W. Zhou, H. Wu, T. Yildirim, J. R. Simpson and A. R. H. Walder, *Phys. Rev. B.*, 2008, **78**, 054114-1; (*b*) Y. Wu, A. Kobayashi, G. J. Halder, V. K. Peterson, K. W. Chapman, N. Lock, P. D. Southon and C. J. Kepert, *Angew. Chem., Int. Ed.*, 2008, **47**, 8929; (*c*) V. K. Peterson, G. J. Kearley, Y. Wu, A. J. Ramirez-Cuesta, E. Kemner and C. J. Kepert, *Angew. Chem., Int. Ed.*, 2010, **49**, 585.

25 L. Kong, G. Román-Pérez, J. M. Soler and D. C. Langreth, *Phys. Rev. Lett.*, 2009, **103**, 096103.

26 P. M. Forster, J. Eckert, B. D. Heiken, J. B. Parise, J.-W. Yoon, S. H. Jhung, J.-S. Chang and A. K. Cheetham, *J. Am. Chem. Soc.*, 2006, **128**, 16846.

27 M. Nielsen, *Phys. Rev. B: Solid State*, 1973, **7**, 1626.

28 N. Nijem, J.-F. Veyan, L. Kong, H. Wu, Y. Zhao, J. Li, D. C. Langreth and Y. J. Chabal, *J. Am. Chem. Soc.*, 2010, **132**, 14834.

29 M. Märcz, R. E. Johnsen, P. D. C. Dietzel and H. Fjellvåg, *Micropor. Mesopor. Mater.*, 2011, DOI: 10.1016/j.micromeso.2011.12.035.